In situ recording of Mars soundscape

S. Maurice, B. Chide, N. Murdoch, R. Lorenz, D. Mimoun, R. C. Wiens, A. Stott, X. Jacob, T. Bertrand, Franck Montmessin, et al.

▶ **To cite this version:**

S. Maurice, B. Chide, N. Murdoch, R. Lorenz, D. Mimoun, et al.. In situ recording of Mars soundscape. Nature, 2022, (in press). 10.1038/s41586-022-04679-0 . insu-03631328v1

HAL Id: insu-03631328

https://insu.hal.science/insu-03631328v1

Submitted on 21 Apr 2022 (v1), last revised 25 Jun 2022 (v2)

HAL is a multi-disciplinary open access archive for the deposit and dissemination of scientific research documents, whether they are published or not. The documents may come from teaching and research institutions in France or abroad, or from public or private research centers.

L'archive ouverte pluridisciplinaire **HAL**, est destinée au dépôt et à la diffusion de documents scientifiques de niveau recherche, publiés ou non, émanant des établissements d'enseignement et de recherche français ou étrangers, des laboratoires publics ou privés.

nature

https://doi.org/10.1038/s41586-022-04679-0

Accelerated Article Preview

In situ recording of Mars soundscape

Received: 7 December 2021

Accepted: 23 March 2022

Accelerated Article Preview
Published online: 01 April 2022

Cite this article as: Maurice, S. et al. In situ recording of Mars soundscape. *Nature* https://doi.org/10.1038/s41586-022-04679-0 (2022)

S. Maurice, B. Chide, N. Murdoch, R. D. Lorenz, D. Mimoun, R. C. Wiens, A. Stott, X. Jacob, T. Bertrand, F. Montmessin, N. L. Lanza, C. Alvarez-Llamas, S. M. Angel, M. Aung, J. Balaram, O. Beyssac, A. Cousin, G. Delory, O. Forni, T. Fouchet, O. Gasnault, H. Grip, M. Hecht, J. Hoffman, J. Laserna, J. Lasue, J. Maki, J. McClean, P.-Y. Meslin, S. Le Mouélic, A. Munguira, C. E. Newman, J. A. Rodríguez Manfredi, J. Moros, A. Ollila, P. Pilleri, S. Schröder, M. de la Torre Juárez, T. Tzanetos, K. M. Stack, K. Farley, K. Williford & the SuperCam team*

This is a PDF file of a peer-reviewed paper that has been accepted for publication. Although unedited, the content has been subjected to preliminary formatting. Nature is providing this early version of the typeset paper as a service to our authors and readers. The text and figures will undergo copyediting and a proof review before the paper is published in its final form. Please note that during the production process errors may be discovered which could affect the content, and all legal disclaimers apply.

ACCELERATED ARTICLE PREVIEW

Article

In situ recording of Mars soundscape

https://doi.org/10.1038/s41586-022-04679-0

Received: 7 December 2021

Accepted: 23 March 2022

Published online: 01 April 2022

S. Maurice[1]✉, B. Chide[2]✉, N. Murdoch[3], R. D. Lorenz[4], D. Mimoun[3], R. C. Wiens[2,5], A. Stott[3], X. Jacob[6], T. Bertrand[7], F. Montmessin[8], N. L. Lanza[2], C. Alvarez-Llamas[9], S. M. Angel[10], M. Aung[11], J. Balaram[11], O. Beyssac[12], A. Cousin[1], G. Delory[13], O. Forni[1], T. Fouchet[7], O. Gasnault[1], H. Grip[11], M. Hecht[14], J. Hoffman[15], J. Laserna[9], J. Lasue[1], J. Maki[11], J. McClean[14], P.-Y. Meslin[1], S. Le Mouélic[16], A. Munguira[17], C. E. Newman[18], J. A. Rodríguez Manfredi[19], J. Moros[9], A. Ollila[2], P. Pilleri[1], S. Schröder[20], M. de la Torre Juárez[11], T. Tzanetos[11], K. M. Stack[11], K. Farley[11], K. Williford[11,21] & the SuperCam team*

Prior to the Perseverance rover landing, the acoustic environment of Mars was unknown. Models predicted that: (i) atmospheric turbulence changes at centimeter scales or smaller at the point where molecular viscosity converts kinetic energy into heat[1], (ii) the speed of sound varies at the surface with frequency[2,3], and (iii) high frequency waves are strongly attenuated with distance in CO_2[2–4]. However, theoretical models were uncertain because of a lack of experimental data at low pressure, and the difficulty to characterize turbulence or attenuation in a closed environment. Here using Perseverance microphone recordings, we present the first characterization of Mars' acoustic environment and pressure fluctuations in the audible range and beyond, from 20 Hz to 50 kHz. We find that atmospheric sounds extend measurements of pressure variations down to 1,000 times smaller scales than ever observed before, revealing a dissipative regime extending over 5 orders of magnitude in energy. Using point sources of sound (Ingenuity rotorcraft, laser-induced sparks), we highlight two distinct values for the speed of sound that are ~10 m/s apart below and above 240 Hz, a unique characteristic of low-pressure CO_2-dominated atmosphere. We also provide the acoustic attenuation with distance above 2 kHz, allowing us to elucidate the large contribution of the CO_2 vibrational relaxation in the audible range. These results establish a ground truth for modelling of acoustic processes, which is critical for studies in atmospheres like Mars and Venus ones.

Prior to Perseverance's landing (Feb. 18, 2021), no pressure fluctuations had ever been monitored on Mars at a frequency > 20 Hz, namely, in the acoustic domain. The recording of sounds offers the unique opportunity to study the atmosphere as the main natural source of sound, and as the propagation medium for acoustic waves. From the knowledge of Mars atmospheric pressure (~0.6 kPa) and the physical properties of CO_2, one can predict (see Methods.1) that: the acoustic impedance results in ~20 dB weaker sounds on Mars than on Earth if produced by the same source, the speed of sound should be around 240 m/s near the surface, and acoustic waves are heavily damped in CO_2 at these atmospheric pressures and temperatures. A few studies[2,3] proposed very detailed models of acoustic propagation on Mars, but with major discrepancies between their results because of a lack of experimental data at low pressure and appropriate temperatures, and the difficulty of characterizing attenuation in a closed environment. Acoustic data are also sensitive to wind speed and direction and, to a lesser extent, other environmental parameters[5,6]. As such, owing to the high sampling frequency of microphones (up to 100 kHz), the acoustic data allow us to explore the atmospheric behavior on a microscale that has never before been accessible on Mars.

The SuperCam instrument suite[7,8] on Perseverance carries an electret microphone, similar to that carried by the Mars Polar Lander[9], lost during atmospheric entry, and the Phoenix spacecraft[10], on which technical issues prevented the device from being operated. SuperCam's microphone is able to record air pressure fluctuations from 20 Hz to 12.5 kHz or 50 kHz, at sampling rates of 25 kHz or 100 kHz respectively. After landing (Martian solar day "Sol" 0; one Sol = 88775 s), the microphone was turned on a first time on Sol 1 while the mast was still stowed. Since

[1]Institut de Recherche en Astrophysique et Planétologie, Université de Toulouse 3 Paul Sabatier, CNRS, CNES, Toulouse, France. [2]Space and Planetary Exploration Team, Los Alamos National Laboratory, Los Alamos, New Mexico, USA. [3]Institut Supérieur de l'Aéronautique et de l'Espace (ISAE-SUPAERO), Université de Toulouse, Toulouse, France. [4]Space Exploration Sector, Johns Hopkins Applied Physics Laboratory, Laurel, Maryland, USA. [5]Earth, Atmospheric, and Planetary Sciences, Purdue University, West Lafayette, Indiana, USA. [6]Institut de Mécanique des Fluides, Univ. Toulouse 3 Paul Sabatier, INP, CNRS, Toulouse, France. [7]Laboratoire d'Etudes Spatiales et d'Instrumentation en Astrophysique, Obs. Paris, CNRS, Sorbonne Univ., Univ. Paris-Diderot, Meudon, France. [8]Laboratoire Atmosphères, Milieux, Observations Spatiales, CNRS, Univ. Saint-Quentin-en-Yvelines, Sorbonne Univ., Guyancourt, France. [9]Universidad de Malaga, Malaga, Spain. [10]Department of Chemistry and Biochemistry, University of South Carolina, Columbia, South Carolina, USA. [11]Jet Propulsion Laboratory, California Institute of Technology, Pasadena, California, USA. [12]Institut de Minéralogie, de Physique des Matériaux et de Cosmochimie, CNRS, Sorbonne Université, MNHN, Paris, France. [13]Heliospace Corporation, Berkeley, California, USA. [14]Haystack Observatory, Massachusetts Institute of Technology, Westford, Massachusetts, USA. [15]Aeronautics and Astronautics, Massachusetts Institute of Technology, Cambridge, Massachusetts, USA. [16]Laboratoire Planétologie et Géosciences, CNRS, Université Nantes, Université Angers, Nantes, France. [17]Escuela de Ingeniería de Bilbao, Universidad del País Vasco UPV/EHU, Bilbao, Spain. [18]Aeolis Corporation, Sierra Madre, California, USA. [19]Centro de Astrobiología (INTA-CSIC), Madrid, Spain. [20]Deutsches Zentrum für Luft- und Raumfahrt (DLR), Institute of Optical Sensor Systems, Berlin, Germany. [21]Blue Marble Space Institute of Science, Seattle, Washington, USA. *A list of authors and their affiliations appears at the end of the paper. ✉e-mail: sylvestre.maurice@irap.omp.eu; bchide@lanl.gov

ACCEPTED ARTICLE PREVIEW

deployment on Sol 2, the microphone is approximately 2.1 m above the ground; it has performed nominally up to the time of writing. SuperCam also consists of a laser-induced breakdown spectroscopy (LIBS) capability to analyze Mars' chemistry at standoff distances from 1.5 to 7 m[7,8]. When the laser pulse interacts with the target, a luminous plasma emits characteristic optical emission lines of the elements present in the target[11]. Plasma expansion generates a shock wave which decouples from the plasma within the first microsecond after laser interaction[12] and results in a clearly detectable acoustic signal[13,14]. Moreover, Perseverance carries a second microphone as part of the Entry, Descent, and Landing Camera (EDLCAM[15]), which has a frequency response from 20 Hz to 20 kHz at a sampling rate of 48 kHz. The EDL microphone is mounted on the port side of the rover, 1 m above the ground. It was activated on Sol 2 and subsequently.

Figure 1 provides an overview of sounds acquired by the SuperCam's microphone (see Methods.2). Sol 38a is the quietest recording in our dataset. Later on that same day (Sol 38b), the power spectral density (PSD) rises above the quiet state at frequencies below 100 Hz. On Sol 117, we associate this rise of power to an increase in the turbulent activity, which extends up to 300 Hz; this is the situation we observe most often. The recording of Sol 148 is the most active one shown, with the same shape starting toward higher frequencies, but with a slope break near 200 Hz; turbulence is detected up to 600 Hz. All non-saturated atmospheric recordings from Sol 0 to Sol 216 fit between the boundaries given by the Sol 38a and Sol 148 spectra. The laser-excited plasma generates a short ~300 µs acoustic pulse (see Methods.6), with 95% of its energy between 3 and 15 kHz. Various spectral notches are caused by acoustic interferences due to echoes from the base of the microphone itself (6 kHz and 12 kHz) or from nearby rocks. The total intensity varies as a function of target distance, as shown for recordings at 2 m, 5 m, and 8 m. During laser-induced spark recording sessions, the atmospheric signal below 1 kHz is masked by electromagnetic interference[8]. The Ingenuity rotorcraft tones (see Methods.3) are also shown.

Atmospheric turbulence

The Martian planetary boundary layer (PBL) is the part of the atmosphere in contact with the surface[16], extending to several km. It is prone to convective turbulence and vertical mixing during daytime, due to the thin atmosphere and low surface thermal inertia that induce strong and unstable near-surface temperature gradients[17–19]. This turbulence translates into high-frequency variations in atmospheric pressure, wind speed, and temperature that can be measured by in-situ instruments. Conversely, during nighttime, the strong radiative cooling of the atmosphere induces highly stable conditions, which efficiently inhibit most convection and turbulence[16]. Probing the PBL at the surface is therefore important to understand how the atmosphere transports and mixes heat, momentum, aerosols and chemical species in the Martian atmosphere[20]. Perseverance's Mars Environmental Dynamics Analyzer instrument (MEDA[21]), and the meteorological suites of previously landed missions[20,22] typically measure pressure, temperature and wind fluctuations with sampling frequencies of 0.1 Hz to 10 Hz. These instruments study the turbulence variability[23,24] and the Martian turbulent energy cascade[1,17,25].

Specifically, we report here on the observation of the dissipative turbulence regime in the PBL, in which the Insight mission could see a hint of a regime change at the limits of the instrument capability[1]. This regime in which molecular viscosity dissipates the turbulent kinetic energy into heat, is now fully characterized by a rapid decrease of the power spectrum with increasing frequency (Figures 1, 2b) over ~5 orders of magnitude. The scale at which the viscous dissipation becomes significant is characterized by the Kolmogorov length scale[26], $\eta = (\nu^3/\varepsilon)^{0.25}$, where ν is the kinematic viscosity, and ε is the turbulence energy dissipation rate per unit mass, typically ~0.001 m^2/sec and 0.005 m^2/sec^3 on Mars, respectively[17]. Thus η ~ 0.02 m and the timescale of these small eddies, $t_\eta = (\nu/\varepsilon)^{0.5}$, is ~0.45 seconds. Hence the dissipation regime should be observable at frequencies above 2 Hz on Mars, at centimeter or smaller scales only (on Earth this transition occurs at millimeter scales or smaller[17]). This theoretical prediction is confirmed by the acoustic data; the threshold moves with frequency, depending on the dissipation rate[25,27]. The balance between energy production and molecular dissipation controls the total amount of turbulent kinetic energy in the boundary layer and, as such, the dissipation mechanism is intrinsically linked to the PBL dynamics; a larger dissipation leads to a more rapid turbulence decay in turn suppressing small-scale wind gustiness, and vice versa.

The microphone records rapid deviations from ambient pressure (> 20 Hz) that are correlated to variations in the wind flow, as shown by Figure 2a where a spectrogram of Sol 38b microphone data (see Methods.5) is overlaid with the wind speed as measured by MEDA (see Methods.4). As expected[6,13], there is a clear correlation between the intensity of acoustic data and the wind speed. This can be due to the flow-induced turbulence from the rover/mast itself but also to the direct sensing of the incoming flow fluctuations, seen to be the dominant factor for outdoor microphones in other studies[6]. Moreover, the daytime local turbulence is known to increase for larger ambient wind speeds[24]. The high microphone sampling rate provides an opportunity to observe very intense but short wind gusts, on a timescale of 10 s. In Figure 2b the same acoustic data are plotted in the frequency domain and combined with low frequency measurements of pressure and wind from MEDA, for a 51-minute time period of continuous data around the microphone acquisition. The large difference in slope between MEDA and microphone data is indicative of regime change. The transition from the likely shear-dominated regime[28] to the dissipation regime occurs in this case between 1 and 20 Hz.

Speed of sound on Mars

In a cold CO_2 atmosphere, the speed of sound is expected to be lower than on Earth. Additionally, due to the low pressure and the physical properties of CO_2, we also expect a dispersion of this speed with frequency[2,3]. On Earth, the adiabatic ratio γ is constant up to a few MHz at ambient pressure[29] and sound speed does not vary with frequency near the surface. At low pressure on Mars, still within the framework of small Knudsen numbers[30] (10^{-6} at 100 Hz to 2.10^{-4} at 20 kHz), the continuum theory still holds, but energy exchanges at molecular scales are modified. Part of the energy associated with the molecules translational motions, which constitute the acoustic waves, is spent on the excitation of inner degrees of freedom (vibrational modes and rotational motions). The relaxation of the rotational motion is almost instantaneous, while relaxation of the vibrational modes occurs over a much longer time scale, a property of small and rigid polyatomic molecules such as CO_2. If the frequency f is smaller than $f_R = 1/\tau_R$, where τ_R is the relaxation time, all modes are equally excited then relaxed. The 7 degrees of freedom that result from 3 translational modes, 2 rotational modes and one doubly-degenerate vibrational mode (ν_2, bending) lead to an adiabatic index $\gamma_0 = 9/7 = 1.2857$. Conversely, if $f > f_R$, there is no time to relax the vibrational mode; in that case there are only 5 active degrees of freedom and $\gamma_\infty = 7/5 = 1.4$. In CO_2 at Earth-ambient pressure, f_R ~40 kHz[31]. This frequency depends on the rate at which molecules can collide, hence f_R is proportional to the pressure. As a result, at 0.6 kPa, the relaxation frequency is about 240 Hz on Mars.

The recording of pulsed waves generated in LIBS mode provides a unique opportunity to measure directly and repetitively the local speed of sound for acoustic waves above 2 kHz, and that is for $f > f_R$ (see Methods.6). From the daytime measurements, sound speeds between 246 m/s and 257 m/s are obtained (Figure 3a), with maximum values between 11:00 to 14:00 Local True Solar Time (LTST) and minimum values around 18:00. The 1σ-dispersion of the sound speed during the ~20 min of a target analysis with LIBS is at its maximum at noon (1.5 %) and is

ACCELERATED ARTICLE PREVIEW

reduced down to 0.5% at 18:00, which highlights the vanishing of the atmospheric turbulence at dusk. These measurements are compared to temperature-derived speeds of sound obtained from (i) the MEDA temperature datasets at the surface, at the height of 0.85 m and 1.45 m, and (ii) the temperature at the surface and at 2 m height given by the Mars Climate Database (MCD[32]) (see Methods.4), using $\gamma_\infty = 1.4$ (since $f > f_R$). The agreement between MEDA and MCD predictions is excellent. SuperCam sound speeds are comparable with temperature-derived values at the level of MEDA's 0.85 m temperature sensor or higher. This is consistent with the fact that the speed is integrated between a height of 2.1 m and the surface, possibly biased toward the surface when the temperature gradient is larger.

Ingenuity's blade passage frequency (BPF)[33] is close to a harmonic source centered around 84 Hz, and in that case for $f < f_R$ (see Methods.3). This signal recorded by SuperCam's microphone is modulated by the variations of the distance range between the microphone and the helicopter. An emitted frequency at 84.43 Hz and a speed of sound $c = 237.7 \pm 3$ m/s are estimated based on a fit of the Doppler effect for flight #4 (see Methods.7). Accounting for the presence of a ~2.5 m/s wind along the microphone-to-helicopter line-of-sight toward the helicopter (MEDA data), the true sound speed is ~240 m/s at this frequency. At the time of the flight, the atmospheric temperatures ranged between 232 K and 240 K at 1.45 m height. Using $\gamma_0 = 1.2857$ (the BPF is below f_R), the temperature-derived speed of sound ranges from 238.8 m/s to 242.9 m/s, which is consistent with the speed directly derived from Ingenuity's flight plus wind (Figure 3b). As a summary, SuperCam's microphone highlights a sound speed dispersion of about 10 m/s in the audible range at the surface of Mars.

Sound attenuation

The most remarkable property of sound propagation on Mars is the magnitude of the attenuation at all frequencies, especially above 1 kHz. The decrease of the LIBS acoustic signal with distance is an opportunity to verify the theory in situ and to test two different attenuation models[3,4] which suffer from a lack of field data at Mars conditions.

As the spherical LIBS acoustic wave propagates, sound pressure decreases as $1/r$ where r is the distance between the target and the microphone. This decrease is scaled by a factor $r^{-0.698}$ to account for the variation of laser irradiance[8], multiplied by $e^{-\alpha r}$ where $\alpha = \alpha(f)$ is the atmospheric attenuation coefficient as a function of frequency. The frequency spectrum of the LIBS acoustic signal is divided into three bands, which account for the three main lobes observed in Figure 1: from 3 kHz to 6 kHz, from 6 kHz to 11 kHz and from 11 kHz to 15 kHz. The evolution of the sound amplitude with distance for the second frequency band is shown in Figure 4a. Over the three bands we find $\alpha = 0.21 \pm 0.04\ m^{-1}$ (95% confidence interval of the fit), $\alpha = 0.21 \pm 0.05\ m^{-1}$, and $\alpha = 0.43 \pm 0.05\ m^{-1}$ respectively. As expected, high pitched sounds are strongly attenuated. Compared to a signal emitted at 1 m, attenuation of an 8 kHz wave ranges from −9 dB at 2 m to −40 dB at 8 m. At 5 m, the atmospheric absorption takes precedence over the geometrical attenuation. On Earth, where $\alpha = 0.01\ m^{-1}$ for the same frequency[34], the attenuation ranges from −6 dB at 2 m to −20 dB at 8 m, and is almost exclusively due to the wavefront spreading. To reach an attenuation of −40 dB on Earth, the source would need to be at 65 m.

Such attenuation coefficients are compared with theoretical[3] and semi-empirical[4] attenuation models in Figure 4b. In situ data tend toward the behavior described by Bass et al[3]. with a plateau at frequencies < 6 kHz then an increase for higher frequencies. Conversely, data do not show an attenuation gap as suggested by the Williams model[4]. This result confirms the large contribution of CO_2 vibrational relaxation in this frequency range, the same process that explains the two values for the speed of sound (above). However, the attenuation coefficient for the 2-6 kHz band is still higher than predicted by Bass et al[3]. It may highlight a different relaxation strength than the one forecasted by the model (see Methods.8). However, these measurements do not reach frequencies low enough to constrain the large discrepancies observed between models below 1 kHz.

Mars Soundscape

Sound is a new, rich source of information on Mars. Thanks to sensors measuring a few millimeters in diameter only, turbulence-induced noise and artificial sources have been recorded. Acoustic waves are governed by the macroscopic thermodynamic properties of fluids (molar mass, heat capacity and temperature, or alternatively compressibility and density). However, given the small displacements and timescales that come into play, we confirm that energy exchanges at the molecular scale also need to be considered to accurately model the sound propagation parameter variations (speed, attenuation) with frequency. More sound speed measurements at different local times and seasons will allow the study of atmospheric fluctuations at a few meters scale on Mars[35–37]. The first in situ retrieval of the acoustic attenuation coefficient already provides new constraints on theoretical models, which are key parameters for geophysical studies in CO_2 dominated atmospheres[38,39]. Wind and turbulence, driven by heat fluxes, are natural sources of pressure fluctuations on Mars. We show that acoustic data yield new insights into the boundary layer turbulence with 10 to 1,000 times higher temporal resolution than before, highlighting for the first time the dissipative regime and a transition to this regime above a few Hz. Characterizing in more details this regime, and the associated transition, is necessary to settle the assumptions used in the numerical modeling of the PBL (including large eddy simulations), telling us what the fraction of missing energy is in the unresolved scales of the models[40,41]. In the future, this will lead to a measurement of the dissipation rate, which is related to the diffusion of heat in the atmosphere, that is currently not well known for Mars[17,42]. Finally, beyond the rumble of the wind, the acoustic signatures of our robotic presence on Mars are rich in information on the health of the rover subsystems.

Online content

Any methods, additional references, Nature Research reporting summaries, source data, extended data, supplementary information, acknowledgements, peer review information; details of author contributions and competing interests; and statements of data and code availability are available at https://doi.org/10.1038/s41586-022-04679-0.

1. Banfield, D. et al. The atmosphere of Mars as observed by InSight. *Nat. Geosci.* **13**, 190–198 (2020).
2. Petculescu, A. & Lueptow, R. M. Atmospheric acoustics of Titan, Mars, Venus, and Earth. *Icarus* **186**, 413–419 (2007).
3. Bass, H. E. & Chambers, J. P. Absorption of sound in the martian atmosphere. *J. Acoust. Soc. Am.* **109**, 3069–3071 (2001).
4. Williams, J.-P. Acoustic environment of the Martian surface. *J. Geophys. Res.* **106**, 5033–5041 (2001).
5. Chide, B. et al. Experimental Wind Characterization with the SuperCam Microphone under a Simulated martian Atmosphere. *Icarus* **354**, 114060 (2021).
6. Morgan, S. & Raspet, R. Investigation of the mechanisms of low-frequency wind noise generation outdoors. *J. Acoust. Soc. Am.* **92**, 1180–1183 (1992).
7. Wiens, R. C. et al. The SuperCam Instrument Suite on the NASA Mars 2020 Rover: Body Unit and Combined System Tests. *Space Sci. Rev.* **217**, 4 (2021).
8. Maurice, S. et al. The SuperCam Instrument Suite on the Mars 2020 Rover: Science Objectives and Mast-Unit Description. *Space Sci. Rev.* **217**, 47 (2021).
9. Delory, G. T., Luhmann, J., Friedman, L. & Betts, B. Development of the first audio microphone for use on the surface of Mars. *J. Acoust. Soc. Am.* **121**, 3116–3116 (2007).
10. NASA - Mars Descent Imager (MARDI), www.nasa.gov/mission_pages/phoenix/spacecraft/mardi.html
11. Miziolek, A. W., Palleschi, V. & Schechter, I. editors. Laser-Induced Breakdown Spectroscopy (LIBS). Cambridge University Press, https://doi.org/10.1017/cbo9780511541261 (2006).
12. Seel, F. Laboratory Studies on Laser-Induced Shock Waves for LIBS Measurements on Mars, Master's, Technische Universität Berlin, https://elib.dlr.de/145677/ (2021).
13. Chide, B. et al. Recording laser-induced sparks on Mars with the SuperCam microphone. *Spec. Acta B: Atomic Spec.* **174** (2020).

ACCEPTED ARTICLE PREVIEW

14. Murdoch, N. et al. Laser induced breakdown spectroscopy acoustic testing of the Mars 2020 microphone. *Planet. Space Sci.* **165**, 260–271 (2019).
15. Maki, J. N. et al. The Mars 2020 Engineering Cameras and Microphone on the Perseverance Rover: A Next-Generation Imaging System for Mars Exploration. *Space Sci. Rev.* **216**, 137 (2020).
16. Savijarvi, H. A model study of the PBL structure on Mars and the Earth. *Contrib. Atmos. Phys.* **64**, 219–229 (1991).
17. Petrosyan, A. et al. The Martian atmospheric boundary layer. *Rev. Geophys.* **49** (2011).
18. Tillman, J. E., Landberg, L. & Larsen, S. E. The Boundary Layer of Mars: Fluxes, Stability, Turbulent Spectra, and Growth of the Mixed Layer. *J. Atmos. Sci.* **51**, 1709–1727 (1994).
19. Larsen, S. E. et al. Aspects of The Atmospheric Surface Layers on Mars and Earth. *Boundary-Layer Meteo.* **105**, 451–470 (2002).
20. Martínez, G. M. et al. The Modern Near-Surface Martian Climate: A Review of In-situ Meteorological Data from Viking to Curiosity. *Space Sci. Rev.* **212**, 295–338 (2017).
21. Rodriguez-Manfredi, J. A. et al. The Mars Environmental Dynamics Analyzer, MEDA. A Suite of Environmental Sensors for the Mars 2020 Mission. *Space Sci. Rev.* **217**, 48 (2021).
22. Banfield, D. et al. InSight Auxiliary Payload Sensor Suite (APSS). *Space Sci. Rev.* **215**, 4 (2019).
23. Ullán, A. et al. Analysis of wind-induced dynamic pressure fluctuations during one and a half Martian years at Gale Crater. *Icarus* **288**, 78–87 (2017).
24. Chatain, A., Spiga, A., Banfield, D., Forget, F. & Murdoch, N. Seasonal Variability of the Daytime and Nighttime Atmospheric Turbulence Experienced by InSight on Mars. *Geophys. Res. Let.* **48** (2021).
25. Temel, O., Senel, C., Spiga, A., Murdoch, N., Banfield, D. & Karatekin, O. Spectral dynamics of the Martian atmospheric turbulence: InSight observations and large-eddy simulations, Submitted to GRL, (2021).
26. Kolmogorov, A. N. The local structure of turbulence in incompressible viscous fluid for very large Reynolds numbers. *Cr. Acad. Sci. URSS* **30**, 301–305 (1941).
27. Chen, W., Lovejoy, S. & Muller, J.-P. Mars' atmosphere: The sister planet, our statistical twin. *J. Geophys. Res.: Atmos.* **121**, 968–11,988 (2016). 11.
28. Tchen, C. M. On the spectrum of energy in turbulent shear flow. *Journal of research of the National Bureau of Standards* **50**, 51–62 (1953).
29. Bass, H. E., Hetzer, C. H. & Raspet, R. On the speed of sound in the atmosphere as a function of altitude and frequency. *J. Geophys. Res.* **112** (2007).
30. Hanford, A. D. & Long, L. N. The direct simulation of acoustics on Earth, Mars, and Titan. *J. Acous. Soc. Am.* **125**, 640 (2009).
31. Zhang, X., Wang, S. & Zhu, M. Locating the inflection point of frequency-dependent velocity dispersion by acoustic relaxation to identify gas mixtures. *Meas. Sci. Technol.* **31**, 115001 (2020).
32. Forget, F. et al. Improved general circulation models of the Martian atmosphere from the surface to above 80 km. *J. Geophys. Res.* **104**, 24155–24175 (1999).
33. Balaram, J., Aung, M. & Golombek, M. P. The Ingenuity Helicopter on the Perseverance Rover. *Space Sci. Rev.* **217**, 56 (2021).
34. Bass, H., Sutherland, L., Piercy, J. & Evans, L. Absorption of sound by the atmosphere. *Phys. acoustics: Principles and Methods* **17**, 145–232 (1984).
35. Noble, J. M. & Auvermann, H. J. The effect of large- and small-scale turbulence on sound propagation in the atmosphere. ARL-TR-565 (1995).
36. Berengier, M. C., Gauvreau, B., Blanc-Benon, P., Juve, D. & de Collongue, G. Outdoor Sound Propagation: A Short Review on Analytical and Numerical Approaches. *Acta Acustica United with Acustica* **89**, 980–991 (2003).
37. Ostashev, V. E. Sound Propagation and Scattering in Random Moving Media, in Sound-Flow Interactions. Editors Aurégan, Y., Pagneux, V., Pinton, J.-F. & Maurel, A. Springer Berlin, Heidelberg, 169-191 (2002).
38. Garcia, R. F. et al. Banerdt. Finite-difference modeling of acoustic and gravity wave propagation in Mars atmosphere: Application to infrasounds emitted by meteor impacts. *Space Sci. Rev.* **211** (2016).
39. Garcia, R. F., Lognonné, P. & Bonnin, X. Detecting atmospheric perturbations produced by Venus quakes. *Geophys. Res. Let.* **32** (2005).
40. Temel, O. et al. Large eddy simulations of the Martian convective boundary layer: Towards developing a new planetary boundary layer scheme. *Atmos. Res.*, 105381 (2021).
41. Spiga, A. et al. A Study of Daytime Convective Vortices and Turbulence in the Martian Planetary Boundary Layer Based on Half-a-Year of InSight Atmospheric Measurements and Large-Eddy Simulations. *J. Geophys. Res. Planets* **126** (2020).
42. Colaïtis, A., Spiga, A., Hourdin, F., Rio, C., Forget, F. & Millour, E. A thermal plume model for the Martian convective boundary layer. *J. Geophys. Res. Planets* **118** (2013).

Publisher's note Springer Nature remains neutral with regard to jurisdictional claims in published maps and institutional affiliations.

© The Author(s), under exclusive licence to Springer Nature Limited 2022

the SuperCam team

R. C. Wiens[2], S. Maurice[1], T. Acosta-Maeda[22], C. Alvarez-Llamas[9], R. B. Anderson[23], S. M. Angel[10], D. M. Applin[24], G. Arana[25], M. Bassas-Portus[3], R. Beal[2], P. Beck[26], K. Benzerara[12], S. Bernard[12], P. Bernardi[7], T. Bertrand[7], O. Beyssac[12], T. Bosak[27], B. Bousquet[28], A. Brown[29], A. Cadu[3], P. Caïs[30], K. Castro[25], B. Chide[2], E. Clavé[28], S. M. Clegg[2], E. Cloutis[24], S. Connell[24], A. Cousin[1], A. Debus[31], E. Dehouck[32], D. Delapp[2], C. Donny[31], A. Dorresoundiram[7], G. Dromart[32], B. Dubois[33], C. Fabre[34], A. Fau[1], W. Fischer[35], O. Forni[1], T. Fouchet[7], R. Francis[11], J. Frydenvang[36], T. Gabriel[23], O. Gasnault[1], E. Gibbons[37], I. Gontijo[11], X. Jacob[6], J. R. Johnson[4], H. Kalucha[35], E. Kelly[22], E. W. Knutsen[8], G. Lacombe[8], N. L. Lanza[2], J. Laserna[9], J. Lasue[1], S. Le Mouélic[16], C. Legett IV[2], R. Leveille[37], E. Lewin[26], G. Lopez-Reyes[38], R. D. Lorenz[4], E. Lorigny[31], J. M. Madariaga[25], M. Madsen[36], S. Madsen[11], L. Mandon[7], N. Mangold[16], M. Mann[31], J.-A. Manrique[1,38], J. Martinez-Frias[39], L. E. Mayhew[40], T. McConnochie[41], S. M. McLennan[42], N. Melikechi[43], P.-Y. Meslin[1], F. Meunier[31], D. Mimoun[3], G. Montagnac[32], F. Montmessin[8], J. Moros[9], V. Mousset[31], N. Murdoch[3], T. Nelson[2], R. T. Newell[2], A. Ollila[2], Y. Parot[1], P. Pilleri[1], C. Pilorget[44,45], P. Pinet[1], G. Pont[31], F. Poulet[44], C. Quantin-Nataf[32], B. Quertier[30], W. Rapin[1], A. Reyes-Newell[2], S. Robinson[2], L. Rochas[31], C. Royer[7], F. Rull[38], V. Sautter[12], S. Schröder[20], S. Sharma[22], V. Shridar[11], A. Sournac[3], A. Stott[3], M. Toplis[1], I. Torre-Fdez[25], N. Turenne[24], T. Tzanetos[11], A. Udry[46], M. Veneranda[38], D. Venhaus[2], D. Vogt[20] & P. Willis[11]

[22]University of Hawaii, Manoa, Hawaii, USA. [23]U.S. Geological Survey, Flagstaff, Arizona, USA. [24]University of Winnipeg, Winnipeg, Canada. [25]University of Basque Country, UPV/EHU, Leioa, Bilbao, Spain. [26]Institut de Planétologie et Astrophysique de Grenoble, CNRS, Univ. Grenoble Alpes, Grenoble, France. [27]Earth, Atmospheric and Planetary Sciences, Massachusetts Institute of Technology, Cambridge, Massachusetts, USA. [28]Centre Lasers Intenses et Applications, CNRS, CEA, Univ. Bordeaux, Bordeaux, France. [29]Plancius Research, Severna Park, Maryland, USA. [30]Laboratoire d'Astrophysique de Bordeaux, CNRS, Univ. Bordeaux, Bordeaux, France. [31]Centre National d'Etudes Spatiales, Toulouse, France. [32]Univ. Lyon, UCBL, ENSL, UJM, CNRS, LGL-TPE, Villeurbanne, France. [33]Groupe d'Instrumentation Scientifique, Observatoire Midi-Pyrénées, Toulouse, France. [34]GéoRessources, CNRS, Univ. Lorraine, Nancy, France. [35]California Institute of Technology, Pasadena, California, USA. [36]University of Copenhagen, Copenhagen, Denmark. [37]McGill University, Montreal, Canada. [38]University of Valladolid, Valladolid, Spain. [39]Agencia Estatal Consejo Superior de Investigaciones Científicas, Madrid, Spain. [40]Department of Geological Sciences, University of Colorado Boulder, Boulder, Colorado, USA. [41]University of Maryland, College Park, Maryland, USA. [42]State University of New York, Stony Brook, New York, USA. [43]Department of Physics and Applied Physics, Kennedy College of Sciences, University of Massachusetts, Massachusetts, USA. [44]Institut d'Astrophysique Spatiale, CNRS, Univ. Paris-Saclay, Orsay, France. [45]Institut Universitaire de France, Paris, France. [46]University of Nevada Las Vegas, Las Vegas, Nevada, USA.

ACCELERATED ARTICLE PREVIEW

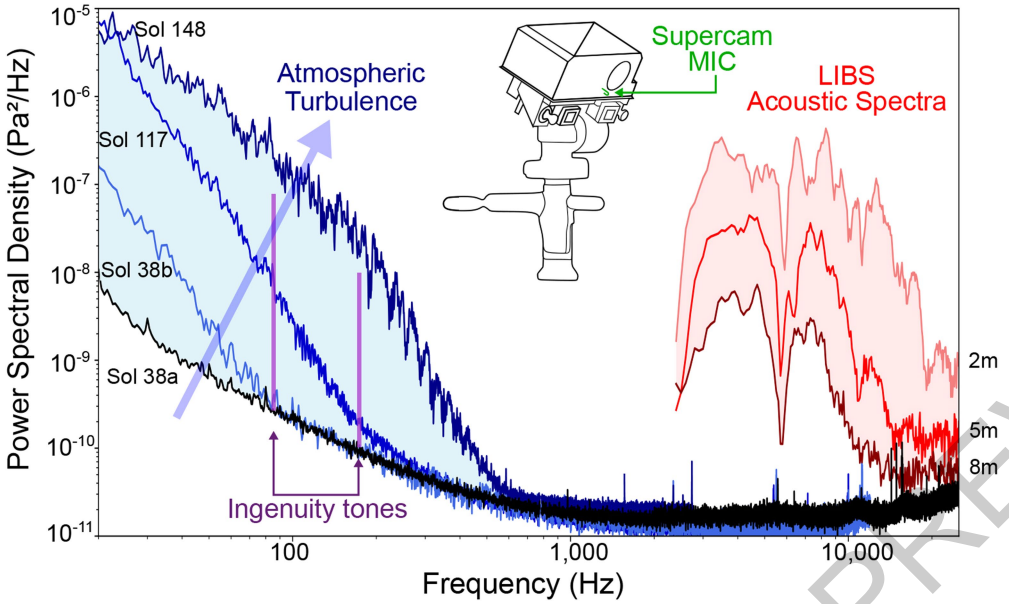

Fig. 1 | Variety of sounds recorded by SuperCam. Atmospheric spectra spread over the light blue area; turbulence increases in the direction of the arrow. LIBS acoustic spectra spread over the light red area. Ingenuity tones are recorded at 84 Hz and 168 Hz (purple). The black spectrum is the quietest recording so far below 1 kHz. SuperCam's microphone is located on the rover mast (green).

ACCELERATED ARTICLE PREVIEW

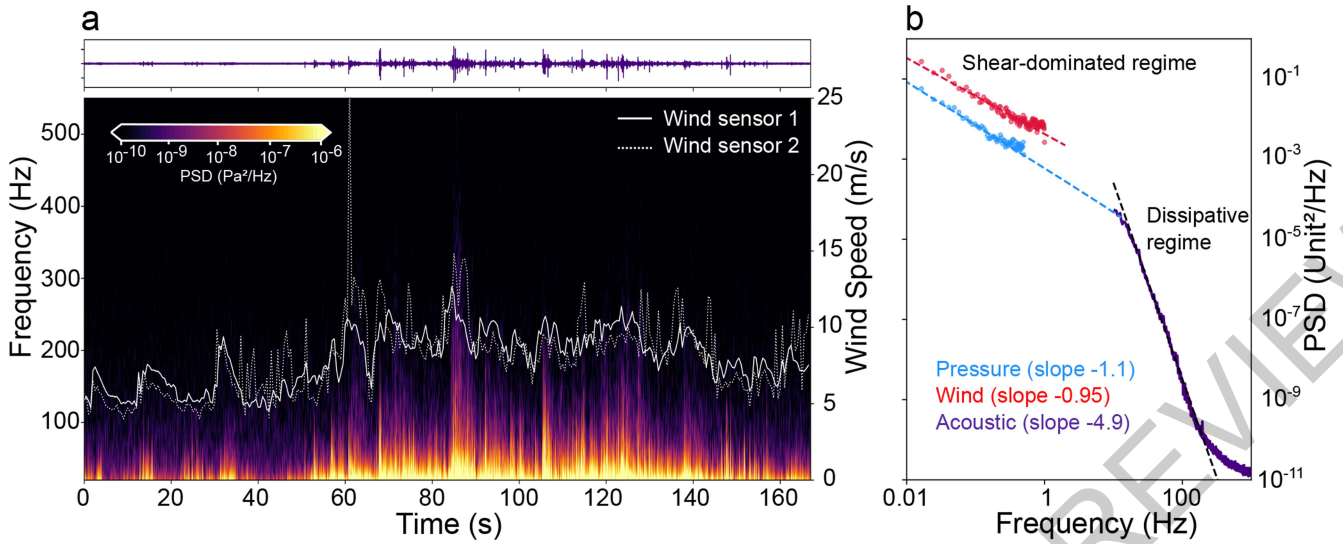

Fig. 2 | Sound recordings and correlation with atmospheric data. Recording of Sol 38b. (a) On top, the y-axis of the time series ranges from −0.2 to 0.2 Pa. The spectrogram (bottom) shows bursts that extend to 300 Hz. Overlaid, with y-axis on the right, are wind speeds from MEDA booms. (b) The PSD calculated for SuperCam's microphone (in Pa^2/Hz over 167 s) and for MEDA pressure (in Pa^2/Hz over 51 min around the microphone acquisition time) and MEDA wind data (in $(m/s)^2/Hz$). The wind PSD is artificially offset by 10^{-2} in the y-axis.

ACCELERATED ARTICLE PREVIEW

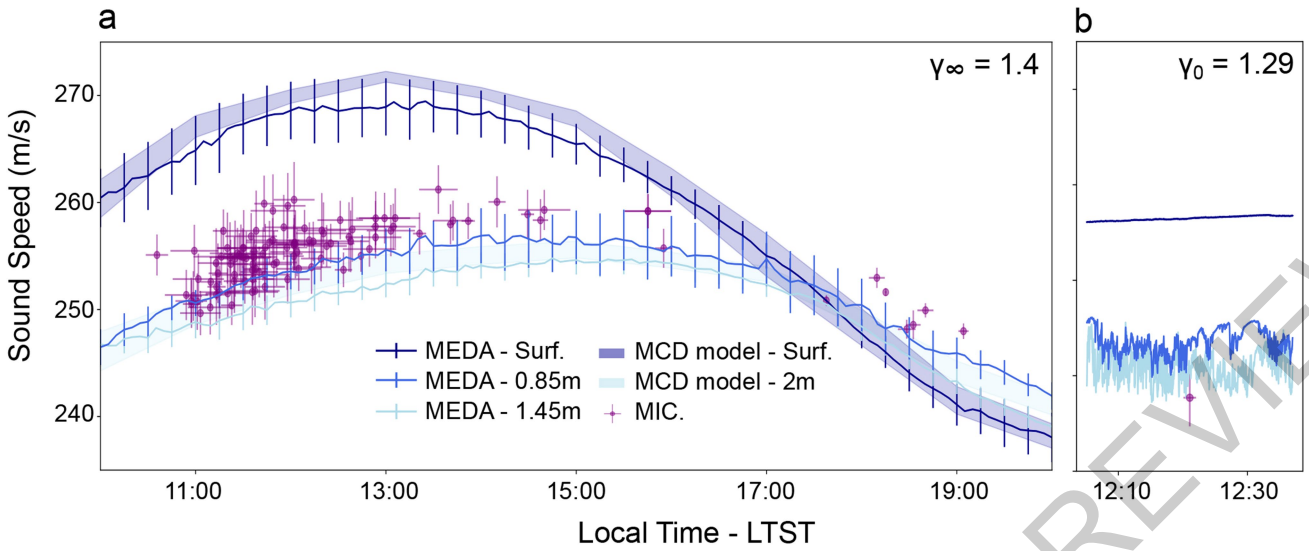

Fig. 3 | Sound speed variations. (**a**) Sound speeds as a function of local time from LIBS time-of-flight data in purple. Other sound speeds are calculated at the 3 heights from MEDA temperatures, at the surface and 2 m altitude from MCD simulations; for these conversions, the adiabatic index above f_R is used. Error bars for MIC data: standard deviation of the sound speeds during each laser burst (vertical), total duration of the burst (horizontal). Error bars for MEDA data: standard deviation of 1-hour bins between Sols 37 and 216. (**b**) Sound speeds are calculated at 3 heights from MEDA temperatures during Ingenuity Flight #4; the adiabatic index below f_R is used. The sound speed estimated from the Ingenuity Doppler effect is in purple. Error bars: 95% confidence interval of the Doppler shift fit.

ACCELERATED ARTICLE PREVIEW

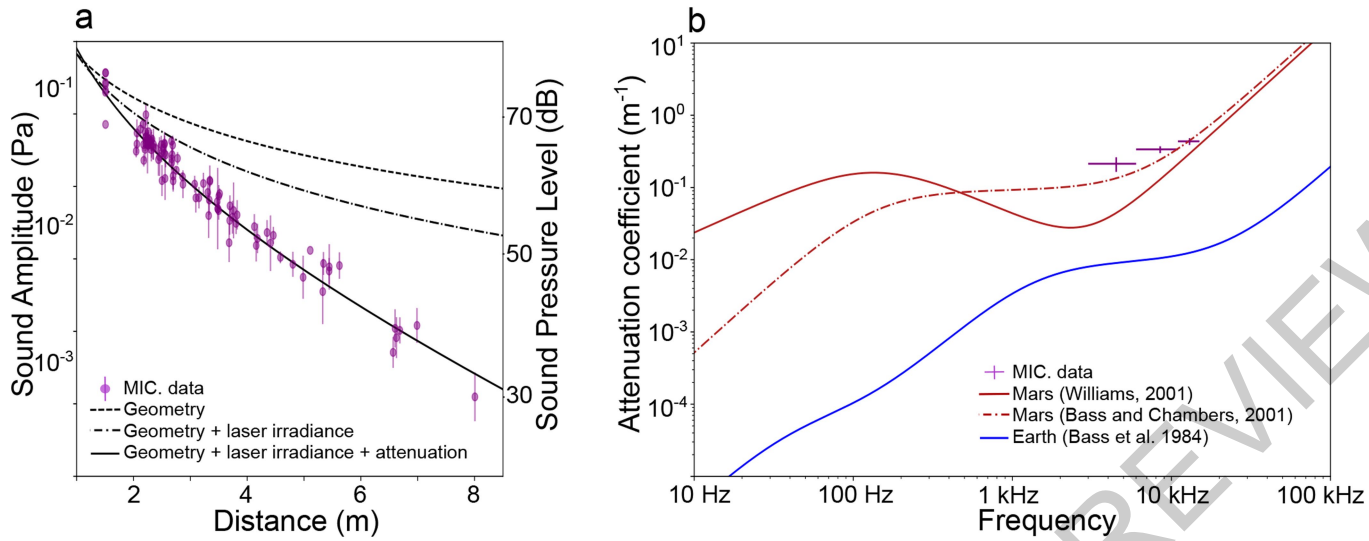

Fig. 4 | Sound attenuation with distance. (**a**) Sound amplitude as a function of target distance r from LIBS acoustic data between 6 kHz and 11 kHz. Second vertical axis on the right for sound pressure level in dB. Signal intensities are in dB relative to 20 µPa. Error bars: standard deviation of the acoustic amplitudes during each laser burst. (**b**) Comparison of the attenuation models for Mars[3,4] (computed at 240 K and 740 Pa) and Earth[34] (293 K and 30% relative humidity). The experimental points correspond to this study. Error bars: 95% confidence interval of the fit done in Fig. 4a (vertical), width of each frequency range (horizontal).

ACCELERATED ARTICLE PREVIEW

Methods

This section starts with a reminder on (1) acoustics adapted to Mars. It provides details of the different datasets: (2) acoustic data from SuperCam's and EDL's microphones; (3) artificial sounds from MOXIE and Ingenuity, in addition to the recording of LIBS shock waves and rover noises; (4) wind speed, temperature, and pressure data from MEDA, temperatures extracted from the Mars Climate Database. Processing methods are presented: (5) computation of power spectral densities; (6) analyses of LIBS shock wave time series; (7) extraction of the Doppler effect from Ingenuity. In the end, (8) supporting explanations on the attenuation with distance are given.

Acoustics reminder

We justify the 3 main assertions in the introduction to the text. (i) The acoustic impedance describes the strength of a medium to sustain acoustic waves. It is given by $Z = \rho c$ in the far field of a source, where ρ is the density and c the speed of sound. Typically, with $\rho = 0.02$ kg/m^3 and $c = 238$ m/s (see below), we obtain $Z = 4.76$ kg.m^{-2}.s^{-1} at the surface of Mars, while $\rho = 1.217$ kg/m^3 and $c = 340$ m/s yield $Z = 413$ kg.m^{-2}.s^{-1}on Earth. This difference of two orders of magnitude translates into signals on Mars being ~20 dB weaker than on Earth when produced by the same source. (ii) At Mars pressure, the ~95% CO_2 atmosphere can be efficiently modeled as an ideal gas. In the microphone frequency range and given the small amplitude of the acoustic pressure, sound waves are considered as adiabatic disturbances. It follows that the temperature-derived speed of sound is given by $c^2 = \gamma RT/M$, with R the molar gas constant (8.314 J mol^{-1} K^{-1}), M the molar mass of the atmosphere (43.34 g.mol^{-1}), T the temperature in Kelvin, and γ the adiabatic index. Using γ=9/7, the standard value for CO_2 – this value is discussed in the main text – we find $c = 238$ m/s at 230 K. (iii) In a rarefied atmosphere, absorption is intrinsically larger as classical (thermal and viscous) and rotational absorption are inversely proportional to the pressure[3]. Moreover, at low frequencies, vibrational absorption dominates over the classical types of absorption, and rotation. It turns out that the vibrational specific heat of CO_2 is 20 times greater than for N_2[3] for a comparison with Earth. Hence, the doubly degenerate mode of CO_2 vibration attenuates sounds at low frequencies, while the viscosity significantly attenuates frequencies higher than a few kHz. Both effects, in terms of attenuation coefficient per meter, are 1 or 2 orders of magnitude stronger than on Earth at the same frequency.

Acoustic dataset

SuperCam's microphone data set used in this study extends from Sol 1 to Sol 216 when the first solar conjunction of the mission occurred. At this date, a total of 4 hours and 40 minutes of Martian sounds have been recorded, including atmospheric turbulence (46% of the total duration), the accompanying pressure waves of LIBS sparks (12%) and mechanical noises (e.g. MOXIE[43], Ingenuity[33], Perseverance's mast rotation, Mastcam-Z mechanisms, 42%). Over the same period, the EDL[15] microphone has recorded a total of 56 minutes of Martian sounds, mainly during rover operations (e.g. rover drive, arm motion). Extended Data Table 1 lists all acoustic files used or mentioned in this study, except for those shown in Figures 3a and 4a which are too many to cite individually (see below).

SuperCam's microphone records air pressure fluctuations from 20 Hz to 12.5 kHz at a 25 kHz sampling frequency, and up to 50 kHz when the 100 kHz sampling mode is used. The analog signal from the microphone, ranging from 0 to 5 V, is digitized (12-bit depth) using one of 4 electronic gains to boost the sensitivity from 0.6 to 21 V/Pa and the resolution from 2 to 0.06 mPa. Gain 0 is used to record the accompanying sounds from LIBS sparks on calibration targets, gains 1, 2, and 3 to record the accompanying sounds from LIBS sparks at various distances, gain 3 for atmospheric recordings. Recordings of the atmosphere and mechanical noises are generally 167 s long. The EDL microphone can record 10 mn and longer time series, with a fixed gain amplifier followed by a 24 bit/44 kHz digitizer (key characteristics are summarized in Extended Data Table 2).

Typical LIBS sequences consist of 30 laser shots at the same position fired at 3 Hz (for technical reasons, only 29 shots are recorded). For a given target, such a sequence is usually repeated from 5 to 10 times, on fresh sampling points separated by a few millimeters. The laser-induced acoustic signal is monitored at a 100 kHz sampling frequency for 60 ms around each laser pulse. The start of the recording window is precisely timed on the laser trigger, so that the propagation time of the sound wave can be measured with an uncertainty < 10 µs. Up to Sol 216, SuperCam's microphone has recorded sound sequences for 123 Martian targets located at distances ranging from 2.05 m (target Garde) to 8.01 m (target Pepin) from the microphone. On seven occasions it has also recorded the acoustic signal related to LIBS measurements of the titanium (Ti) calibration target[44] located on the rover deck at 1.51 m from the microphone.

For the derivation of the sound speed (Figure 3a), targets farther than 6 m are excluded because of a small signal-to-noise ratio that prevents a good time-of-flight measurement. Recordings of the LIBS acoustic signals from Ti are also excluded as their sound propagates above the rover and are biased by extra heating and turbulence induced by the warm body of the rover. In total, 109 targets between Sol 1 and Sol 216 are considered for Figure 3. For the attenuation study (Figure 4), regolith or loose material targets, which generally lead to a lower sound amplitude, are excluded, as well as out-of-focus points for the same reason. In total 96 targets are used. The measurements from Ti are included and provide a useful constraint on the attenuation at short distance. As the laser energy used on Ti is lower than the laser energy used on Mars targets (110 A pumping current on Ti compared to 155 A on Mars targets), the PSD amplitude from the Ti measurements are normalized by a factor 155/110 as the pumping current is proportional to the laser energy, which is proportional to the laser irradiance, as the spot size and the pulse duration remains the same.

Dataset of artificial sounds

Both EDL and SuperCam microphones are also used to record sounds produced by the rover. They help to inform operators about equipment health (e.g. rover driving, Mars oxygen in-situ resource utilization experiment - MOXIE) and provide sources of sound that are well localized in space and time (e.g. during Ingenuity flights or LIBS sparks). All recordings also pick up some perturbations such as intense single-frequency emissions at 195 Hz, 198.75 Hz and the following harmonics at 780 Hz and 795 Hz that are due to the rover internal heat pump used for thermal management. Sounds of the rover's instruments or pumps propagate through both structural vibrations (microphonics) and acoustic propagation in the atmosphere.

The EDL microphone[15] was used to record the rover drive on Sol 16 (Extended Data Fig. 1a). Broad quasi-continuous "screech" signals in the 520-700 Hz, 1.2-1.4 kHz, and 1.6-1.9 kHz bandwidths are assumed to arise directly from frictional interaction of the metal wheel tread with surface rocks. Sonorous transients or "clanks" are seen at 13 s with several narrow frequency components, but with a lower total sound intensity than the aforementioned phenomenon. It is hypothesized that these are structural resonances of mobility system elements (e.g. suspension) excited by near-impulsive changes in loading, e.g. when a wheel slips off the edge of a rock.

The Ingenuity rotorcraft[33] provides a localized but moving source of sound on Mars. On Sol 69 during flight #4, SuperCam's microphone recorded the entire 116 s duration of the flight. A prominent acoustic signal, up to 2.10^{-7} Pa^2/Hz (1.5 mPa sound pressure level), associated with the blade passage frequency (BPF) at 84 Hz and its first overtone 168 Hz was detected by SuperCam's microphone (Extended Data Fig. 1b). All phases of the flight are visible, but the takeoff occurred during a gust (at the rover location) as high as 20 mPa. The BPF clearly stands out

ACCEPTED ARTICLE IN REVIEW

but its overtone is much fainter, due to greater atmospheric absorption at higher frequency. After landing, the microphone captured the blades spinning down.

The MOXIE instrument[43] operates every 1-2 months to produce a few grams of gaseous O_2. The primary objective of these repeated operations is to look for possible degradation of the O_2 production efficiency associated with the harsh environment of Mars. MOXIE utilizes SuperCam's microphone recordings for independent diagnosis of compressor performance, including precise measurements of the motor rotation rates as indicated by the fundamental frequency of the observed comb of harmonics. Distinct transitions in Extended Data Fig. 1c, recorded during a nighttime run (Sol 81), correspond to commanded changes in motor speed from 50 to 58.3 Hz. The loudest harmonics are near 500 Hz, where several additional frequencies are also excited. This range corresponds to resonant frequencies of the MOXIE instrument, as observed during dynamics testing. Even recorded during one of the quietest times of the day, the amplitude of the signal only reaches 1.5 mPa.

Recording LIBS sparks was the main rationale to develop SuperCam's microphone to infer physical properties of rock targets, such as their hardness[13]. Typical LIBS sequences consist of 30 laser shots at the same position per observation, fired at 3 Hz (Extended Data Fig. 1d). LIBS operations are monitored by the microphone at a 100 kHz sampling rate for 60 ms around each laser pulse. The mean amplitude of the signal is 0.25 ± 0.08 Pa (1σ) for this shot sequence.

Wind speed, temperature, and pressure data

The wind, temperature and pressure data are recorded from the Mars Environmental Dynamics Analyzer (MEDA[21]) instrument. The wind data are acquired up to 2 Hz, pressure at 1 Hz and temperature at 1 or 2 Hz. Wind speed and direction are independently acquired from two separate booms separated by 120° (termed boom 1 and boom 2) where one is preferred for a given wind direction (see accuracies and resolutions in Extended Data Table 2).

The Mars Climate Database[32] (MCD) provides climate predictions derived from 3D simulations of Mars atmosphere performed with the Mars global climate model developed at the Laboratoire de Météorologie Dynamique (http://www-mars.lmd.jussieu.fr). The LMD Mars GCM is described in ref. [32], but since then it has adopted more sophisticated and realistic modeling for the CO_2, dust and water cycles, photochemistry, radiative transfer, etc. In this work, we use the climatology scenario[45] from the MCD Version 5.3, in which (i) the simulated spatial and vertical dust distributions are reconstructed from observations over the Martian Years 24 to 31 without global dust storms (thus representative of standard climate conditions), and (ii) average solar EUV conditions are assumed. In this study, the MCD outputs (surface temperature and atmospheric temperature at 2 m above surface) are provided for daytime local times in increments of 1 hr, and between Ls=5.2° and Ls=104.7° in increments of 10° to capture the seasonal variations in temperature.

Spectral analysis of acoustic data

SuperCam's microphone data are converted from Volts to Pascals using the instrument sensitivity for each gain (0.6, 1.3, 5.3, and 21.6 V/Pa, corresponding to amplification factors of 29 to 972). The microphone's electronic response function for each gain (band-pass filter between 100 Hz and 10 kHz) is used to correct raw spectra below 100 Hz and above 10 kHz. EDL microphone data are not converted into physical units. PSD represented in Figures 1 and 2b were computed from a Fourier transform, using a Welch's estimator. Spectrograms represented in Figures 2a, Extended Data Fig. 1b and 1c are computed with a Hanning window of 2 s. Extended Data Fig. 1a is computed with a window of 1 s and Extended Data Fig. 1d with a window of 5 ms.

Time series (Laser-induced spark recordings)

The creation of the laser-induced plasma is accompanied by a shock wave, which can be described as an N-wave acoustic pulse[46] primarily, a short ~300 µs long compression/rarefaction acoustic signal. This signal is followed by echoes on nearby rocks and the rover structure, plus diffraction. The whole acoustic signal lasts typically less than 5 ms. A band-pass filter is applied to remove electromagnetic interferences, atmospheric signal below 2 kHz, and to reduce noises above 20 kHz. There are residuals of the laser warmups, but they do not affect the determination of the sound speed (Extended Data Fig. 2).

Time series data are used to calculate the local speed of sound. The distance to each target, which is returned by the instrument's autofocus, is known to an accuracy of ±0.5%[8]. The laser trigger time is known to a few microseconds and the shock wave becomes sonic after 1 µs[12], which is less than 0.1% of the propagation time. The arrival of the pressure wave is considered to be detected when the signal rises 3σ above the background.

Doppler effect (Ingenuity recording)

Ingenuity flights #4 (Sol 69), #5 (Sol 76), #6 (Sol 91) and #8 (Sol 120) were recorded by SuperCam at 25 kHz sampling rate. We use Flight #4 data, since this flight came closer to Perseverance than any other flight SuperCam could record. During this flight, Ingenuity climbed to an altitude of 5 m, accelerated to 3.5 m/s, traveled 130 m at constant height, decelerated, turned around, and returned to its base by the same route. Taking off at 76 m distance from Perseverance, it came as close as 69 m, and has moved as far as 123 m from Perseverance (Extended Data Fig. 3b, bottom).

On the PSD obtained over the whole recording, the Blade Passage Frequency (BPF, 2x the rotation rate for a 2-bladed rotor) at 84 Hz and its first harmonic at 168 Hz are clearly visible above the background, which itself is higher than that of Sol 38a, a very quiet recording on Mars (Extended Data Fig. 3a). There is no other tone above the background. There is a period of atmospheric turbulence up to 56 s into the recording that explains why the spectrum at low frequency is above that of Sol 38a. Discontinuities in the amplitude of the tones at 84 Hz and 168 Hz are visible during the cruise phase of the flight. Such a modulation beat is due to the interferences of 2 signals with slightly different frequencies (~50 mHz apart), each originating from the two blades that are frequency shifted. The study of this phase shift is outside the scope of this paper.

Each tone is fitted by a Gaussian function every 0.5 s. We report in the main text on the study the BPF at 84 Hz. The received frequency varies along Ingenuity's flight (Extended Data Fig. 3b, top) as a function of the variation of the distance range between the rover and the helicopter. The received frequency, the classical Doppler effect, varies by ±1.5 %. The fit of this tone, when the atmosphere is quiet (t > 60 s), as a function of the range rate, yields f = 84.44 Hz for the BPF at the source, and c = 237.7 ±3 m/s. A similar fit to the first harmonic yields f = 168.90 Hz and c = 236.9 ±4 m/s, that is coherent with values derived from the BPF.

Sound attenuation with distance

As the sound wave propagates through an atmosphere, part of the acoustic energy is transferred to the propagation medium as heat by an absorption mechanism called atmospheric (or intrinsic) attenuation. This process has been largely described and validated for the Earth atmosphere[34,47,48]. The atmospheric attenuation, linked to the motion of molecules, depends on the frequency of the wave. It can be attributed to two phenomena: (i) the classical attenuation includes the heat loss caused by viscous friction and losses from non-adiabatic heat diffusion between the compression and rarefaction areas. This phenomenon is all the more important for short period waves, when there is less time to establish an equilibrium. The classical attenuation is proportional to the square of the frequency. (ii) The molecular attenuation, due to the excitation of the internal degrees of freedom of the polyatomic molecules (rotational and vibrational modes), each one taking some time, called "relaxation time", to return to equilibrium. The shorter the period of the wave is, compared to the relaxation time, the less time molecules have to relax their energy, and hence the greater is the absorption of the acoustic energy.

ACCEPTED ARTICLE IN PREVIEW

This theory has been applied to Mars' atmosphere to compute empirical attenuation models[3,4] (Figure 4). Although Mars models are in good agreement above 10 kHz (classical attenuation is well constrained thanks to a good knowledge of dynamic viscosity and thermal conductivity for CO_2 as a function of temperature), they differ significantly in the infrasonic and part of the audible range, depending on the way molecular relaxation is modeled. The Williams model[4] extrapolates experimental data for CO_2 that have been acquired at 1 bar and above 273 K. The model considers that molecular attenuation increases proportionally to the frequency, reaches a maximum value at the relaxation frequency, f_R (240 Hz) and then decreases as $1/f$. On the other hand, the Bass and Chambers model[3] discriminates molecular relaxation into rotational and vibrational relaxations. Rotational relaxation is modeled by f squared, just like classical attenuation. For vibrational relaxation, the model considers that below f_R, vibrational attenuation grows as f squared. Above f_R, vibration modes are not excited and the vibrational attenuation stays at a constant level.

As a supplementary note, CO_2 has 3 vibrational modes at 1,341 cm^{-1} (ν_1 symmetric stretching), 667 cm^{-1} (ν_2 degenerate bending), and 2,349 cm^{-1} (ν_3 asymmetric stretching). Associated vibrational temperatures are 1,890 K, 960 K and 3,360 K, respectively. At 240 K, the respective contribution of each mode to the vibrational specific heat are 3.7% (ν_1), 96.3% (ν_2) and < 0.1% (ν_3) at 240 K. This justifies why first-order models can only consider the contribution of the ν_2 bending mode to the vibrational specific heat.

Data Availability

All acoustic data are publicly available at the Planetary Data System Geosciences Node. https://doi.org/10.17189/1522646.

43. Hecht, M. et al. Mars Oxygen ISRU Experiment (MOXIE). *Space Sci. Rev.* **217**, 9 (2021).
44. Manrique, J. A. et al. SuperCam Calibration Targets: Design and Development. *Space Sci. Rev.* **216**, 138 (2020).
45. Millour, E. et al. The Mars Climate Database (Version 5.3). Scientific Workshop: From Mars Express to ExoMars, 27-28 February 2018, ESAC Madrid, Spain.
46. Chiba, R., Ishikawa, Y., Hasegawa, J. & Horioka, K. Time evolution of laser-ablation plumes and induced shock waves in low-pressure gas. *Physics of Plasmas* **24**, 063520 (2017).
47. Qin, Q. & Attenborough, K. Characteristics and application of laser-generated acoustic shock waves in air. *App. Acous.* **65**, 325–340 (2004).
48. Sutherland, L. C. & Bass, H. E. Atmospheric absorption in the atmosphere up to 160 km. *J. Acous. Soc. Am.* **115**, 1012–1032 (2004).

Acknowledgements Many other people helped with this project in addition to the co-authors, including hardware and operation teams, and we are most grateful for their support. This project was supported in the US by the NASA Mars Exploration Program, and in France is conducted under the authority of CNES. The work of A. Munguira is supported by the grant PID2019-109467GB-I00 funded by MCIN/AEI/10.13039/501100011033.

Author contributions S.M. and B.C. led equally the writing of the manuscript. S.M., B.C., N.M., R.L., A.S., X.J., T.B., and F.M. performed data processing and interpreted the data. D.M. is the lead of SuperCam's microphone, R.W. the lead of SuperCam investigation, N.L. and B.C. the leads of SuperCam acoustic working group. Other investigations provided data and support to this study: J.M. is the lead of EDL's microphone; M.A., J.B., H.G., and T.T. are leading the Ingenuity project; M.H., J.H., and J.MC. are leading the MOXIE investigation; JA.RM., M.T., and C.N. are leading the MEDA investigation and mission atmospheric working group. All other co-authors provided helpful comments and inputs to the manuscript. The SuperCam team built the instrument, helps daily to operate it, to process, and interpret the data.

Competing interests The authors declare no competing interests.

Additional information
Correspondence and requests for materials should be addressed to S. Maurice or B. Chide.
Peer review information *Nature* thanks Andi Petculescu, Roger Waxler and Peter Read for their contribution to the peer review of this work.
Reprints and permissions information is available at http://www.nature.com/reprints.

ACCELERATED ARTICLE PREVIEW

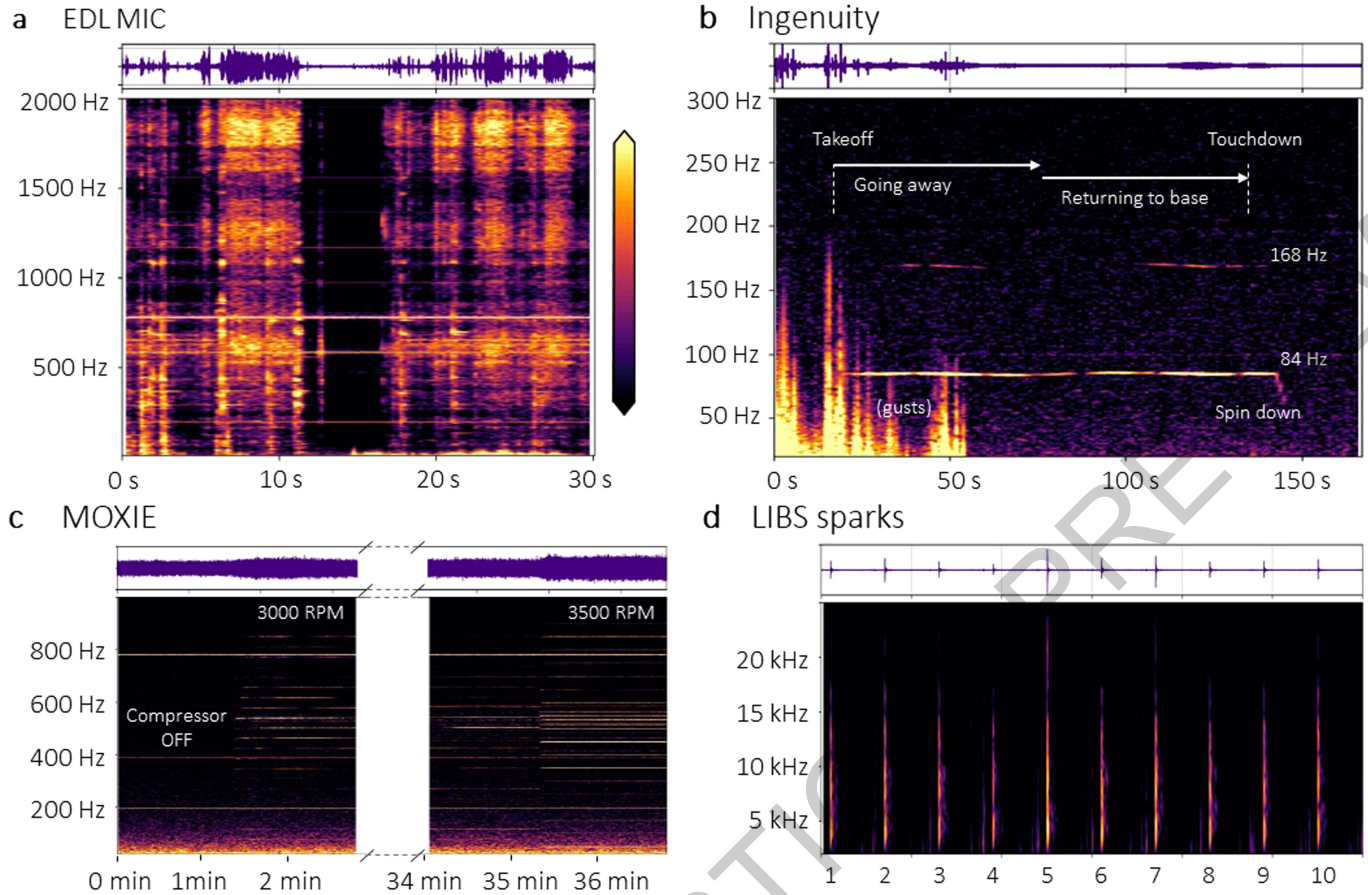

Extended Data Fig. 1 | Artificial sounds recorded by Perseverance. For each panel: time is along the x-axis; on top time series data in mPa (see hereafter for the range when it exists); at the bottom PSD in Pa^2/Hz (a color-scale is shown next to panel a; ranges are different for each panel, but not indicated). (a) Unfiltered spectrogram of a segment (240 – 270 s) of the 16-minute EDL microphone record during the rover drive (Sol 16). Time series data are not calibrated in pressure. (b) Spectrogram of Ingenuity Flight 4 (Sol 69). Time series data range from −10 mPa to +10 mPa. (c) Unfiltered spectrogram of MOXIE oxygen production (Sol 81). Time series data range from −2.5 mPa to +2.5 mPa. (d) Series of 10 LIBS shots on target Hedgehog (Sol 37), labeled one-to-ten. Time series data range from −500 mPa to 500 mPa.

ACCELERATED ARTICLE PREVIEW

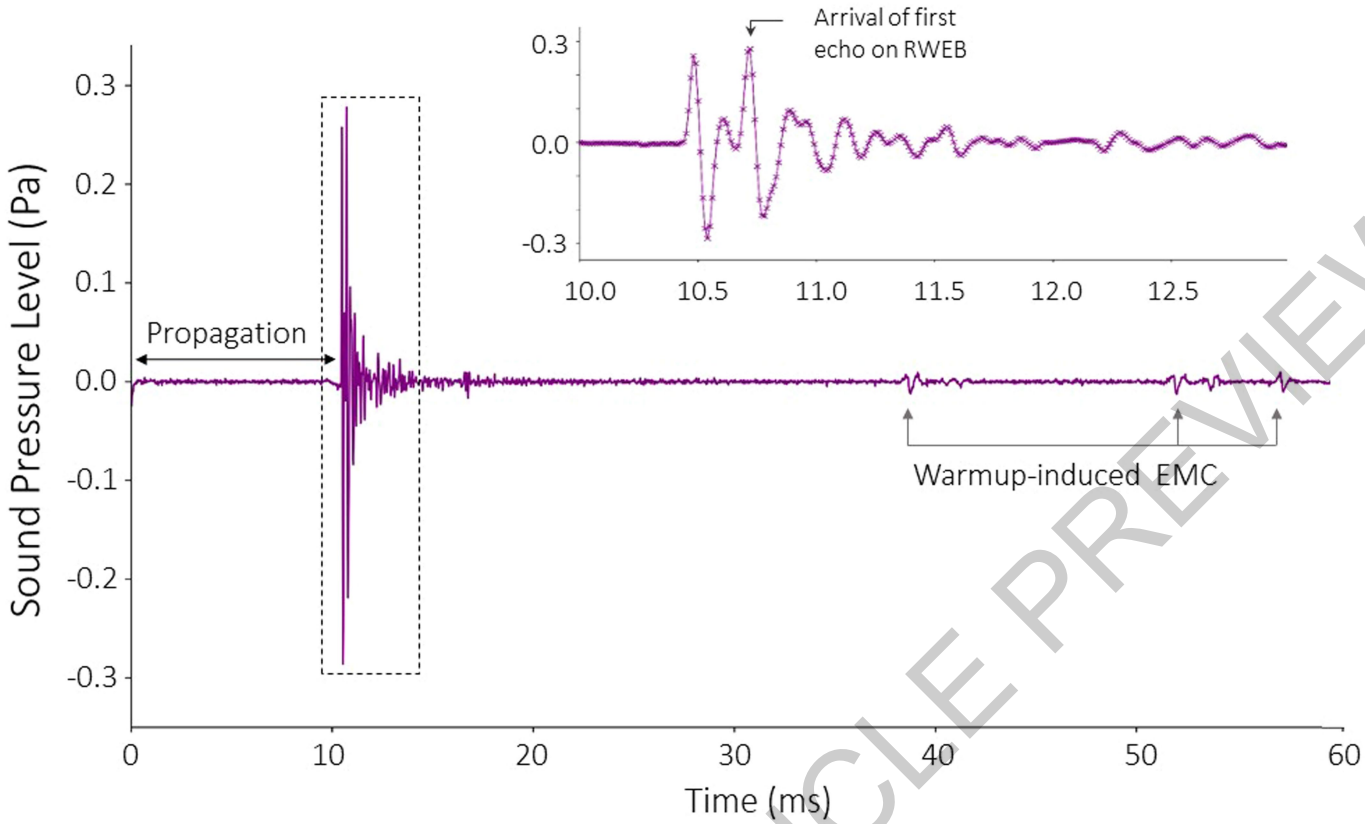

Extended Data Fig. 2 | Recording of laser-induced shock wave. Target Hedgehog (point #1, shot #1). The inset focuses on the time when the acoustic wave is recorded.

ACCELERATED ARTICLE PREVIEW

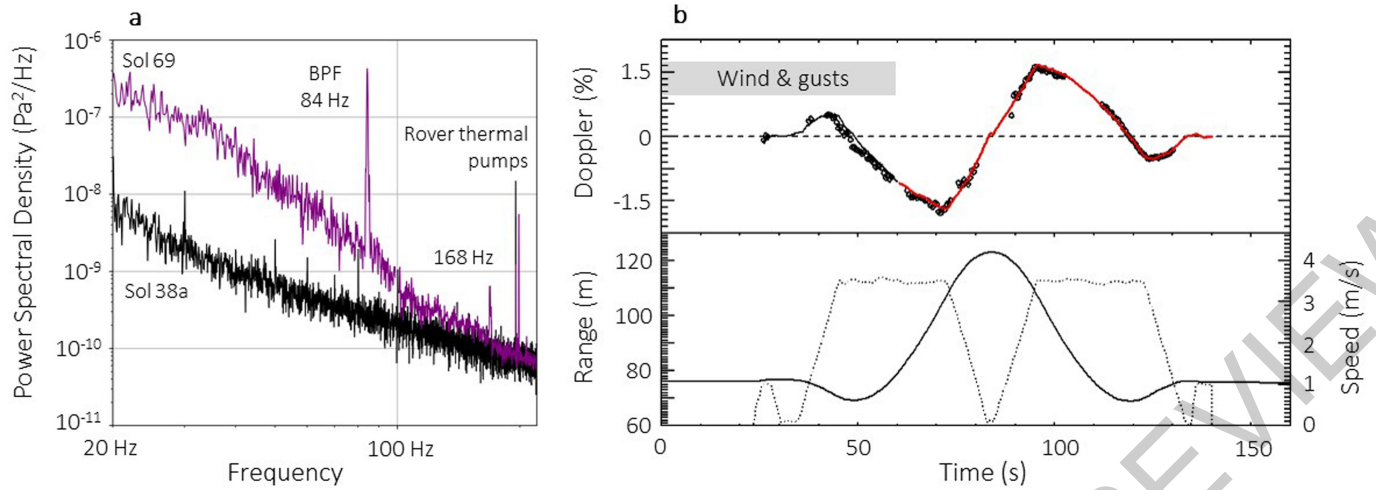

Extended Data Fig. 3 | Recording of Ingenuity flight #4 Blade Passage Frequency. (a) PSD over the entire recording (purple). The rover's thermal pumps show at 195 Hz and 198.75 Hz. PSD for Sol 38a is the reference of a quiet day. (b) Top: variations of the received frequency along the trajectory of the flight (diamond symbol). During the first 60 s, the recording is perturbed by high winds. In red the Doppler effect is modeled with f = 84.44 Hz at the source and c = 237.7 m/s. Bottom: Range between the rover and Ingenuity (solid line, left y-axis) and rotorcraft speed (dotted line, right y-axis).

ACCELERATED ARTICLE PREVIEW

Extended Data Table 1 | List of audio recordings used in this study

Acquisition time		LTST	Type of recording	Sampling frequency	Notes
Sol 1	(S)	13:50	Atmosphere	100 kHz	First sounds by SuperCam with mast stowed
Sol 2	(E)	10:07	Atmosphere	48 kHz	First sounds by ELDCam
Sol 4	(S)	16:14	Atmosphere	100 kHz	First sounds by SuperCam with mast deployed
Sol 16	(E)	16:50	Rover drive	48 kHz	Mobility (ED Fig. 1a)
Sol 37	(S)	11:51	LIBS sparks	100 kHz	Target Hedgehog, 29 recordings (ED Fig. 1d and Fig. 2)
Sol 38a	(S)	11:53	Atmosphere	25 kHz	Quietest atmosphere (Fig. 1, ED Fig. 3)
Sol 38b	(S)	15:49	Atmosphere	25 kHz	Low turbulence atmosphere (Fig. 1, 2)
Sol 69	(S)	12:19	Ingenuity	25 kHz	Flight #4 (ED Fig. 1b and Fig. 3a)
Sol 72	(S)	17:13	LIBS sparks	100 kHz	SCCT Ti, series of 10 shots at 1.51 m (Fig. 4a)
Sol 81	(S)	04:30	MOXIE	25 kHz	Compressor (ED Fig. 1c)
Sol 108	(S)	11:16	LIBS sparks	100 kHz	Target Jih at 5 m (Fig. 1)
Sol 117	(S)	12:24	Atmosphere	25 kHz	Average atmosphere (Fig. 1)
Sol 147	(S)	11:10	LIBS sparks	100 kHz	Target Pepin, farthest distance at 8.01 m (Fig. 1)
Sol 148	(S)	12:10	Atmosphere	25 kHz	Very active atmosphere (Fig. 1)
Sol 209	(S)	10:58	LIBS sparks	100 kHz	Target Garde, closest distance 2.05 m (Fig. 1)

Recordings from SuperCam's (S) and EDL's (E) microphones, with the Local True Solar Time (LTST) of each acquisition.

ACCELERATED ARTICLE PREVIEW

Extended Data Table 2 | Origin and characteristics of dataset used in this study

Value	Payload element	Key characteristics	Ref.
Pressure fluctuations	SuperCam microphone 4 electronic gains, ~2.1 m height	20 Hz – 12.5 kHz (or) 50 kHz Gain 0: 0 – 8.3 Pa, Resolution 2 mPa Gain 3: 0 – 0.24 Pa, Resolution 0.06 mPa	7, 8
Pressure fluctuations	EDL microphone 1 m height	20 Hz – 20 kHz Not calibrated (arb. units)	15
Air temperatures	MEDA Air Temperature Sensors (ATS) 0.84 m and 1.45 m height	Sampling 1 Hz (or) 2 Hz Accuracy < ±1 K Resolution < ±0.01 K	21
Static Pressure	MEDA Pressure Sensor (PS) ~1 m height	Sampling 1 Hz Accuracy < ±5 Pa Resolution ±0.12 Pa	21
Ground temperature	MEDA Thermal Infrared Sensor (TIRS) Surface	Sampling 1 Hz Accuracy ±0.75 K Resolution ±0.08 K	21
Wind speed and direction	MEDA Wind Sensor (WS) 2 booms, 120° apart, 1.5 m height	Sampling 1 Hz (or) 2 Hz Accuracy ±1 m/s (up to 10 m/s), 10% over 10 m/s Resolution ±0.5 m/s (up to 10 m/s), 10% over 10 m/s Direction ±15°	21

Audio recordings are provided by SuperCam and EDL microphones. Atmospheric data are provided by MEDA. Resolution and accuracy are defined as the 90%-confidence range of the statistical error of the pressure, temperature, or wind speed values[8,21].

ACCELERATED ARTICLE PREVIEW